ADVANCED FUNCTIONAL MATERIALS
www.afm-journal.de

Materials Views
www.MaterialsViews.com

Core/Shell PbSe/PbS QDs TiO_2 Heterojunction Solar Cell

Lioz Etgar, Diana Yanover, Richard Karel Čapek, Roman Vaxenburg, Zhaosheng Xue, Bin Liu, Mohammad Khaja Nazeeruddin, Efrat Lifshitz, and Michael Grätzel*

Quasi type-II PbSe/PbS quantum dots (QDs) are employed in a solid state high efficiency QD/TiO_2 heterojunction solar cell. The QDs are deposited using layer-by-layer deposition on a half-micrometer-thick anatase TiO_2 nanosheet film with (001) exposed facets. Theoretical calculations show that the carriers in PbSe/PbS quasi type-II QDs are delocalized over the entire core/shell structure, which results in better QD film conductivity compared to PbSe QDs. Moreover, PbS shell permits better stability and facile electron injection from the QDs to the TiO_2 nanosheets. To complete the electrical circuit of the solar cell, a Au film is evaporated as a back contact on top of the QDs. This PbSe/PbS QD/TiO_2 heterojunction solar cell produces a light to electric power conversion efficiency (η) of 4% with short circuit photocurrent (J_{sc}) of 17.3 mA/cm^2. This report demonstrates highly efficient core/shell near infrared QDs in a QD/TiO_2 heterojunction solar cell.

1. Introduction

The development of quantum dot (QD) based solar cells is growing fast including nanocrystal (NC)-polymer hybrid solar cells, NC-Schottky solar cells, NC-sensitized titanium dioxide (TiO_2) solar cells, and NC hybrid bilayer solar cells.[1–8] More recently, heterojunction PbS QD solar cells have been published,[9–14] which steered a rapid increase in the performance of the QD based solar cells. Multiple exciton generation (MEG) effect was also demonstrated in similar cell structures.[12,15,16] PbSe and PbS QDs have large ground state absorption cross sections (≈10–15 cm^{-2}), and relatively large exciton Bohr radii, 46 nm for PbSe and 20 nm for PbS. In addition their band gap can be tuned from 0.3 to 2.0 eV.[17–19]

Core/shell QDs offer the possibility of a partial and internal charge separation and a better chemical stability. In type-I QDs, a wide-gap semiconductor coats a core made of a narrower-gap material; in this case both the electron and hole reside in the same part of the heterostructure (the QD core). In type-II QDs, there is alignment of energy states at the interface between two semiconductors, which encourages spatial separation of electrons and holes between two regimes. In quasi type-II, at least one of the carriers is delocalized over the entire core/shell structure.[20–22] In particular, in PbSe/PbS of a small size, both carriers are delocalized over the entire core/shell structure, due to the small potential barrier at the core/shell interface, however, with different spread of the wavefunction across the interface. Thus, slight carriers' separation is achieved, still the option to extract both carriers away from the exterior surfaces of the QDs.

Here, we report on solid state PbSe/PbS-based QD/TiO_2 heterojunction solar cells. Within such a cell, the PbSe/PbS QDs act as an absorber and at the same time as a hole conductor. We studied the core/shell composition by X-ray photoelectron spectroscopy (XPS), and calculated their electron and hole wave functions. It was observed that both carriers are delocalized over the entire core/shell structure; therefore, facile charge separation was achieved. This PbSe/PbS QD/TiO_2 heterojunction solar cell achieved high current density of 17.3 mA cm^{-2} and a light to electric power conversion efficiency (PCE) of 3.93% under 0.9 sun intensity, importantly these PbSe/PbS QD/TiO_2 heterojunction solar cells achieved PCE of 4.7% under 0.1 sun intensity.

2. Results and Discussion

Figure 1 presents HR-TEM images of 2.5 nm PbSe core QDs and its size distribution (Figure 1A,C) and PbSe/PbS core/shell QDs and its size distribution with size of 3.5 nm (Figure 1B,D).

The samples were studied by XPS in order to analyze their composition. **Figure 2** presents an XPS spectrum of the core/shell sample (PbSe/PbS), magnified around the binding energies of the three relevant elements. Based on the XPS data it was possible to calculate the PbS shell thickness which coated the PbSe core using the relation:

$$\frac{\frac{4}{3}\pi(r_{cs}-r_c)}{\frac{4}{3}\pi r_c} \cong \frac{S}{Se} \quad (1)$$

Dr. L. Etgar
Institute of Chemistry
The Hebrew University of Jerusalem
Jerusalem, 91904, Israel
E-mail: lioz.etgar@mail.huji.ac.il
Dr. L. Etgar, Dr. M. K. Nazeeruddin, Prof. M. Grätzel
Department of Sciences and Chemical Engineering
École Polytechnique Fédérale de Lausanne- EPFL, Lausanne, 1015, Switzerland
D. Yanover, Dr. R. K. Čapek, R. Vaxenburg, Prof. E. Lifshitz
Schulich Faculty of Chemistry
Solid State Institute
Russell Berrie Nanotechnology Institute
Grand Technion Energy Program, Technion, Haifa 32000, Israel
Z. Xue, Prof. B. Liu
Department of Chemical and Biomolecular Engineering
National University of Singapore, Singapore

DOI: 10.1002/adfm.201202322

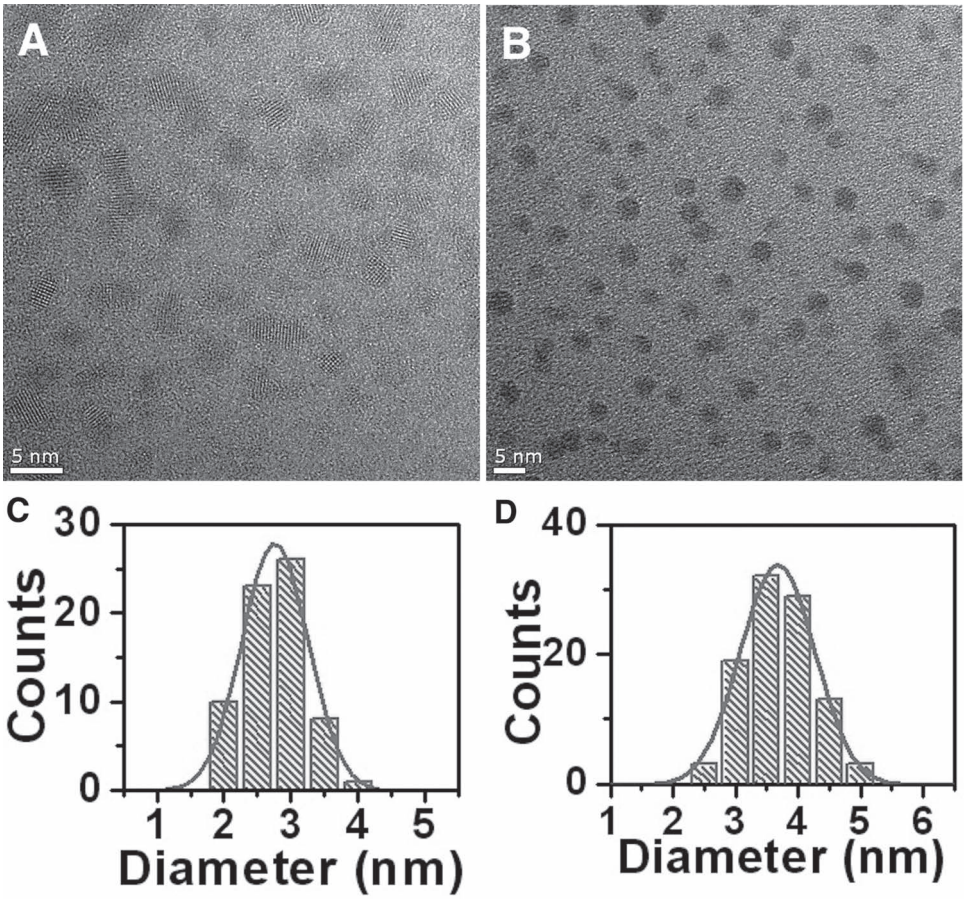

Figure 1. HR-TEM images of A) PbSe core with diameter of 2.5 nm and B) PbSe/PbS core/shell with a diameter of 3.5 nm. C,D) Size distribution of the PbSe core (C), and of the PbSe/PbS core/shell (D).

where r_{cs} is the exterior core/shell radius and r_c is the core radius, S and Se are the atomic percentage of sulfur and selenium, respectively. The PbSe core diameter in the core/shell sample is 2.5 nm. The core sizes were calculated according to their excitonic peak absorbance.[23]

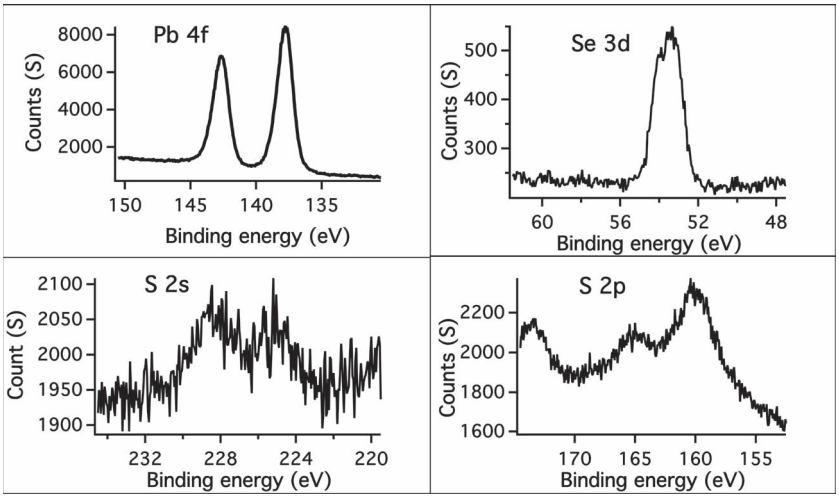

Figure 2. XPS spectra of PbSe/PbS core/shell sample with shell thickness of 0.5 nm. The three different elements can be observed.

Table 1 presents the XPS data and the calculated shell thickness for the studied samples. The HR-TEM and XPS data supplied the option to calculate the PbS monolayers coated the PbSe core. The lattice parameter of PbS is equal to 0.594 nm,[24] which suggest that in this case the PbS shell is close to one monolayer (one unit cell).

The absorbance spectra of the PbSe core and the PbSe/PbS core/shell sample are shown in **Figure 3**, showing a pronounced exciton ($1S_h$–$1S_e$) transition. The exciton peak positions are listed in Table 1.

To learn about the electronic structure of the core and core/shell QDs, the following calculations were preformed. The electronic structure of the core and core/shell QDs was calculated in the framework of the four-band k·p envelope function theory,[25] which describes the electronic properties of the IV–VI semiconductors in the vicinity of the four equivalent L-points of the first Brillouin zone. Spin-orbit coupling, band-edge effective mass anisotropy, and spatial variation of the

Table 1. XPS data for PbSe core and PbSe/PbS core/shell samples.

Sample	Eg [eV]	Excitonic peak absorbance [nm]	XPS (Atomic%)			Shell thickness [nm]
			Pb	Se	S	
PbSe core	1.63	760	79.6	20.6	–	–
PbSe/PbS	1.29	960	59.65	14.65	25.7	0.5

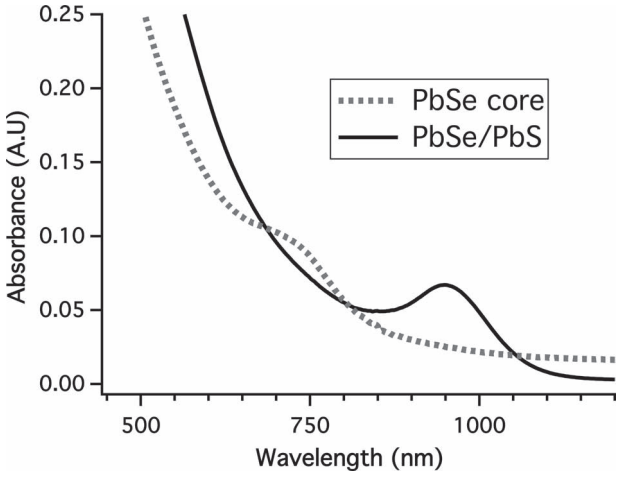

Figure 3. Absorbance spectra of the PbSe core and the PbSe/PbS core/shell sample.

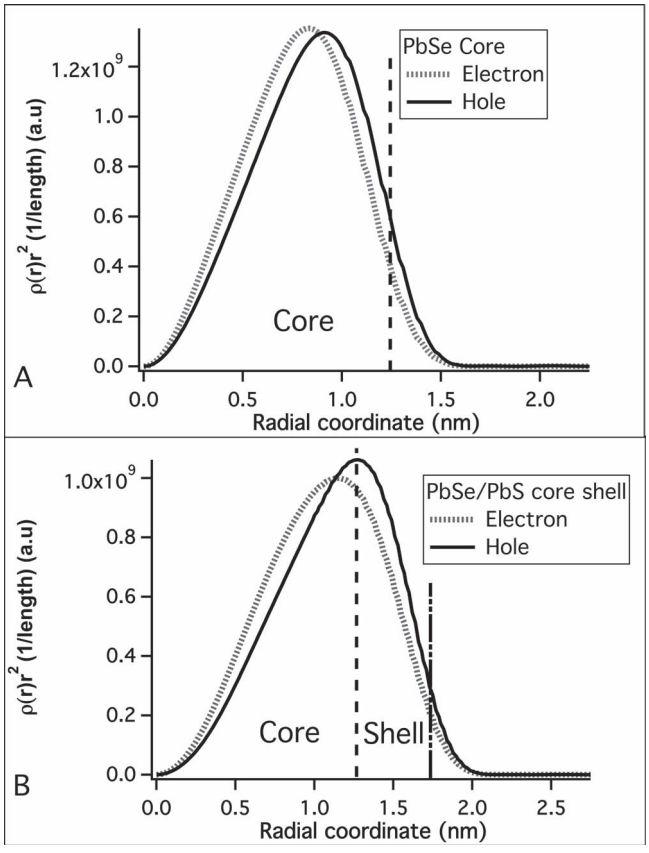

Figure 4. Electron and hole wave functions for A) core PbSe QDs and for B) core/shell PbSe/PbS QDs. The vertically dashed lines represent the core border and the shell border.

material parameters are adequately accounted for in the model.[26]

The energy zero is conveniently chosen at the vacuum level and the band-offsets taken in the case of PbSe/PbS core/shell QDs are 0.155 and 0.025 eV for the conduction and valence bands, respectively. The Hamiltonian is numerically diagonalized in the basis of spherical harmonics and zero-order Bessel functions, yielding the single-particle energy levels and wavefunctions discussed below.

The radial distribution function of the electron and hole in the PbSe core QDs and the PbSe/PbS core/shell QDs as a function of the radial coordinate can be seen in **Figure 4**. Within the PbSe core, the electron and hole wave functions (Figure 4A) are delocalized, however interestingly in the PbSe/PbS core/shell structure, both carriers are delocalized over the entire core/shell structure with nearly identical degree of delocalization, permitting extraction of both carriers and potential improvement of carrier transport through QDs-films.

The QDs described above were used for the fabrication of QD/TiO_2 hetrojunction solar cells. The structure of the cell is similar to one described in our previous work.[12,13] The working electrode of such hetrojunction solar cells was composed of TiO_2 nanosheets, the top and bottom facets of the nanosheets are the (001) planes. The nanosheets consisted of well-defined rectangular sheet-like structures with a side length of 30 nm and a thickness of 7 nm. Full characterization of the (001) TiO_2 nanosheets is described in our previous work.[12]

Figures 5 presents a scheme of the device structure and its corresponding energy level diagram. The bottom layer is composed of compact TiO_2 and TiO_2 nanosheets with exposed (001) facets layers acting as electron collectors. PbSe QDs or PbSe/PbS core/shell QDs were deposited on top of the TiO_2 nanosheets film using a layer-by-layer deposition technique. The QD film should absorb the light. The original ligands of the QDs (oleic acid) were exchanged by mercaptopropionic acid (MPA) during deposition. A gold contact was evaporated on top of the QD film.

The operation mechanism of the PbSe/PbS core/shell QD/TiO_2 heterojunction solar cell (presented in Figure 5) shows a depletion layer that can extend from the TiO_2 nanosheets film to the QD film.[12,14] The local electric field present in the depletion layer is essential in assisting the separation of photogenerated electron-hole pairs.

Table 2 summarizes the results obtained for cells made from core PbSe QDs and core/shell of PbSe/PbS QDs. It is seen from the table, that the core/shell PbSe/PbS QDs-based device showed a better performance than that based on the core PbSe QDs. The PbS shell cover the PbSe core provides sufficient protection from a oxidation, thus, providing the PbSe/PbS QDs with chemical and photo-chemical stability. The best performance was achieved using PbSe/PbS core/shell QDs with a PbS

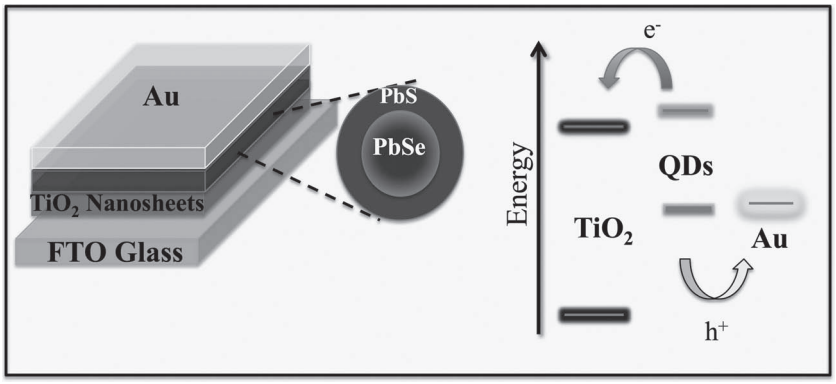

Figure 5. Scheme of the heterojunction solar cell using PbSe QDs or PbSe/PbS QDs. The energy level diagram of the QD heterojunction solar cell is shown on the right.

Table 2. Photovoltaic results of the PbSe QDs and the PbSe/PbS core shell measured at 0.9 sun intensity.

Sample	V_{oc} [mV]	J_{sc} [mA/cm^2]	Fill Factor (FF)	η [%]
PbSe core	411.34	5.22	0.31	0.74
PbSe/PbS	474.58	17.36	0.429	3.93

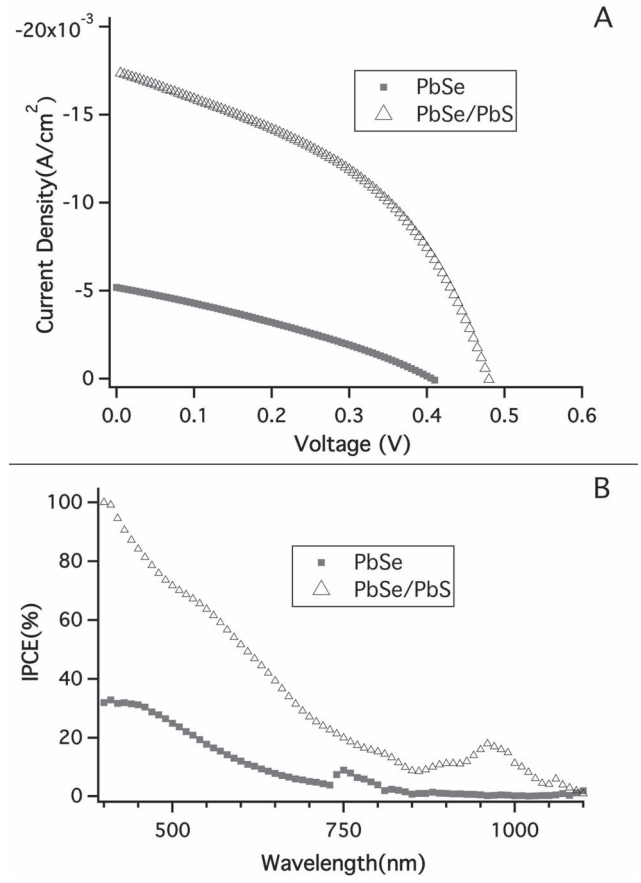

Figure 6. A) Comparison of the *J–V* characteristics for the solid state PbSe and PbSe/PbS QDs device. A mask with aperture area of 0.12 cm^2 was placed over the device. B) IPCE spectra of the PbSe and PbSe/PbS QD/TiO_2 heterojunction solar cell.

shell of 0.5 nm (corresponding to about 1 PbS monolayers) and a band gap of 1.29 eV.

Figure 6A presents the photovoltaic results obtained for core PbSe QDs and core/shell PbSe/PbS QDs listed in Table 2. We obtained the best performance with QDs having a diameter of 3.5 nm (first excitonic peak at 960 nm, E_g = 1.29 eV). These PbSe/PbS QDs produce an open-circuit voltage (V_{oc}) of 0.474 V, a short circuit current density (J_{sc}) of 17.3 mA cm^{-2} and a fill factor (FF) of 43%, corresponding to power conversion efficiency (PCE) of 3.93% under 0.9 sun intensity, while the photovoltaic performance under 0.1 sun intensity showed a J_{sc} of 2.39 mA cm^{-2}, a FF of 48%, corresponding to a PCE of 4.7%.

Figure 6B shows the incident photon to current conversion efficiency (IPCE), which specifies the ratio of extracted electrons to incident photons at a given wavelength. The IPCE spectra are plotted as a function of wavelength of the light. The solid state QD cell shows a good response from the visible through the near infrared (NIR), all IPCE spectra show response at the position of the excitonic peak of the corresponding QDs. The IPCE using the PbSe/PbS core/shell is reaching its maximum of 100% at 400–420 nm. The PbSe/PbS core/shell QDs located close to the TiO_2 interface absorb most efficiently the photons at these wavelengths. The excitonic peak of the PbSe/PbS QDs is observed at 960 nm corresponding to an IPCE of 18%. Integration of the IPCE spectrum over the AM1.5 solar emission yields a photocurrent density of 17.6 mA/cm^2, in good agreement with the measured values.

Studies of PbSe/PbS QDs suggest quasi type-II heterostructure, with good alignment between the core and the shell.[27] According to our theoretical calculations (Figure 4A,B), the exciton wave function of the PbSe/PbS core shell QDs is not localized within the PbSe core as expected. Instead, the wave functions of both carriers extend over the entire structure, in a similar close manner to core QDs. In the case of PbSe/PbS QDs discussed in this work, the wave function extend into the shell and ignore the material boundary. This results in efficient electron injection from the core/shell QDs to the TiO_2 nanosheets and to better conductivity of the QD film. Recent examination of photochemical stability of the discussed QDs (to be published elsewhere), indicated chemical stability of the core/shell PbSe/PbS QDs upon a short term (30 min) to oxygen, suggesting removal of oxidation surface sites, thus, eliminating carriers' surface trapping, which should allow smooth charge extraction in a solar cell. Such a stability does not exist in core PbSe QDs, that tends to be oxidized immediately upon oxygen exposure. Thus, the core/shell QDs offered here, supply chemical and photochemical stability, as well as higher degree of charge extraction.

This work uses the PbSe QDs as a case study; the energy levels, HOMO and LUMO, can be changed in respect to the potential of the electrodes. This paves the way to extend the absorbance of the heterojunction solar cell into the IR regime where the PbS QDs are not active.

3. Conclusions

PbSe core and PbSe/PbS core/shell QDs were synthesized and employed in a QD/TiO_2 heterojunction solar cell. The best photovoltaic performance was achieved using a 0.5-nm PbS shell (corresponding to around 1 of PbS layer) having a diameter of 3.5 nm with E_g of 1.29 eV. The photovoltaic parameters give a J_{sc} of 17.3 mA/cm^2, a V_{oc} of 0.474 V, a FF of 0.43 corresponding to a solar to electric power conversion efficiency (η) of 3.93% under 0.9 light intensity. Theoretical calculations showed that the wave functions of electrons and holes are extended to both materials, which contribute to the better photovoltaic performance than the PbSe core. The PbS shell cover the PbSe core should provide sufficient protection from a fast-oxygen penetration, thus, providing the PbSe/PbS QDs with low surface trapping, chemical and photo-chemical stability, contributed to the success of their integration into solar cell device.

4. Experimental Section

PbSe Core Synthesis: The reaction mixture, consisting of 1.6 mmol PbO, 4.8 mmol oleic acid (OA), 6.4 mmol stearyl alcohol and hexadecane (HDC) (when the total mass of the reaction mixture was adjusted to 8 g by adjustment of the amount of HDC) was heated to 100 °C under vacuum in a 25 mL three necked flask for 1 hour. Under a nitrogen atmosphere, the temperature was adjusted to the particular injection temperature. The selenium precursor solution, containing 2.3 g pure trioctyl phosphine (TOP) Se, 0.95 g diphenylphosphine (DPP) and HDC (when total volume injection solution was 4 mL) was then injected into the reaction mixture. The temperature was reduced to the growth temperature of 70 °C. To quench the reaction and to perform the first precipitation, the flask was opened at standard atmosphere and the reaction mixture was poured into a mixture of ethanol, acetonitrile, and toluene (volume ratio of 3:3:4). The QDs were separated by centrifugation. It should be noted that the QDs were supposed to be protected during the first precipitation against oxidation due to unreacted phosphine. Therefore, for the second precipitation, the test tube was transferred to a nitrogen filled glove box. Further, care was taken that the colloid or precipitate did not come into contact with oxygen in the following steps. The test tube was opened, and the supernatant was removed. The precipitate was then dissolved in hexane, and the two-fold volume (relative to the hexane) of acetonitrile was added. A two-phase system formed, while the QDs were present in the hexane phase. The four-fold volume (relative to the hexane) of ethanol was subsequently added drop-wise, which caused the disappearance of the second phase and a precipitation of the QDs. The mixture was kept aside for 16 h and the precipitate was separated again by centrifugation. Then, the supernatant was removed, while the precipitate was dried under a nitrogen atmosphere and finally dissolved in hexane under a nitrogen atmosphere.

PbSe/PbS Core/Shell Synthesis: lead acetate trihydrate and oleic acid (1:8 lead to OA) in 5 mL of diphenylether were heated at 160 °C under vacuum for 1 h. The temperature was lowered to 70 °C and the purified PbSe cores were added to the reaction mixture. Then, bis(trimethylsilyl) sulfide (TMS_2S) diluted in diphenylether was drop-wise injected to the reaction mixture. Purification of the obtained core/shell QDs was done twice by precipitation with acetone. More detailed synthetic procedure can be found in ref.[29] The PbSe and PbSe/PbS QDs were stored in nitrogen glove box.

X-ray photoelectron spectroscopy (XPS) measurements were performed in a Thermo VG Scientific Sigma Probe fitted with a monochromotized X-ray Al Kα (1486.6 eV) source. Data analysis was performed using the Sigma Probe Advantage software.

High resolution transmission electron microscope (HR- TEM) image was recorded with a Tecnai F20 G^2 instrument operated at 300 kV. The absorption spectra were recorded using a JASCO V-570 UV-vis-NIR spectrometer.

Synthesis and Purification of TiO_2 Nanosheets: The synthesis of the nanosheets followed a typical experimental procedure.[30] Ti(OBu)4 (10 mL, 98%) and hydrofluoric acid (0.8 mL, 47%) solution mixed in a 150 mL dried Teflon autoclave was kept at 180 °C for 24 h to yield the TiO_2 nanosheets. After the reaction was cooled to room temperature, the white powder was separated by high-speed centrifugation and washed with ethanol followed by distilled water for several times.

Methods and Device Fabrication: During device fabrication, a thin blocking layer of compact TiO_2 was first deposited by spray pyrolysis onto a pre-cleaned FTO glass substrate using a solution of titanium diisopropoxide bis(acetylacetonate) in ethanol as precursor. Subsequently, a nanosheet TiO_2 layer was deposited by spin coating (3000 rpm for 10 s) from a dilute aqueous solution containing a mixture of TiO_2 nanosheets and ethanol (volume ratio of 1:3). This results in a nanosheet titania film with 300 ± 50-nm thickness. The procedure for deposition of the QD film is similar to the one reported in our previous work.[12] The QDs were subsequently deposited layer-by-layer on the porous TiO_2 film by spin coating a 50 mg mL^{-1} solution in octane. Each layer was cast at a spinning rate of 2500 rpm applied for 10 s and treated thereafter briefly with a solution of 10% 3-mercaptopropionic acid (MPA, ≥99.0% from Sigma–Aldrich) in methanol using again 2500 rpm rotational speed for 10 s. This treatment displaced the oleate ligand and rendered the QD insoluble, which allowed thin films of 300-nm thicknesses to be created using 12 successive deposition cycles. Each layer was rinsed with anhydrous methanol (purchased from Sigma–Aldrich) to remove excess of MPA and QDs. Finally, a gold back contact of ≈100-nm thickness was deposited by evaporation through a shadow mask. The device was then completed by encapsulation in an argon atmosphere. The encapsulation of the device was made by placing 2-mm glass on top of the active area of the device using a frame of hot melt Surlyn (25-μm thick) as a sealant and spacer. After encapsulation, the device was stable in ambient air.

Photovoltaic Characterization: Photovoltaic measurements employed an AM 1.5 solar simulator equipped with a 450 W xenon lamp (model 81172, Oriel). Its power output was adjusted to match AM 1.5 global sunlight (100 mW/cm^2) by using a reference Si photodiode equipped with an IR-cutoff filter (KG-3, Schott) in order to reduce the mismatch between the simulated light and AM 1.5 (in the region of 350–750 nm) to less than 2% with measurements verified at two PV calibration laboratories [ISE (Germany), NREL (USA)]. *I–V* curves were obtained by applying an external bias to the cell and measuring the generated photocurrent with a Keithley model 2400 digital source meter. The voltage step and delay time of photocurrent were 10 mV and 40 ms, respectively. A similar data acquisition system was used to determine the monochromatic incident photon- to-electric current conversion efficiency. Under full computer control, light from a 300 W xenon lamp (ILC Technology, USA) was focused through a Gemini-180 double monochromator (Jobin Yvon Ltd., U.K.) onto the photovoltaic cell under test. The monochromator was incremented through the visible spectrum to generate the IPCE (λ) as defined by IPCE (λ)) = 1240($J_{sc}/\lambda\phi$), where λ is the wavelength, J_{sc} is the short-circuit photocurrent density (mA cm^{-2}), and ϕ is the incident radiative flux (mW cm^{-2}). Photovoltaic performance was measured by using a metal mask with an aperture area of 0.12 cm^2.

Acknowledgements

We acknowledge the European Community's Seventh Framework Programme (FP7/2007–2013) under grant agreement no. 246124 of the SANS project, and the Global Research Laboratory (GRL) Program for financial support. L.E. acknowledges the Marie Curie Actions—Intra-European Fellowships (FP7-PEOPLE-2009-IEF) under grant agreement no. 252228, project "Excitonic Solar Cell". B. Liu thanks L'Oreal-Singapore Women in Science National Fellowship 2011 for financial support.

Received: August 14, 2012
Revised: November 18, 2012
Published online: December 27, 2012

[1] J. M. Luther, M. Law, M. C. Beard, Q. Song, M. O. Reese, R. J. Ellingson, A. J. Nozik, *Nano Lett.* **2008**, *8*, 3488.
[2] W. Ma, J. M. Luther, H. Zheng, Y. Wu, A. P. Alivisatos, *Nano Lett.* **2009**, *9*, 1699.
[3] R. Plass, S. Pelet, J. Krueger, M. Grätzel, U. Bach, *J. Phys. Chem. B* **2002**, *106*, 7578.
[4] B. Sun, A. T. Findikoglu, M. Sykora, D. J. Werder, V. I. Klimov, *Nano Lett.* **2009**, *9*, 1235.
[5] J. M. Luther, M. Law, Q. Song, C. L. Perkins, M. C. Beard, A. J. Nozik, *ACS Nano* **2008**, *2*, 271.
[6] S. Zhang, P. W. Cyr, S. A. McDonald, G. Konstantatos, E. H. Sargent, *Appl. Phys. Lett.* **2005**, *87*, 233101.
[7] B.-R. Hyun, Y.-W. Zhong, A. C. Bartnik, L. Sun, H. D. Abruňa, F. W. Wise, J. D. Goodreau, J. R. Matthews, T. M. Leslie, F. Borrelli, *ACS Nano* **2008**, *2*, 2206.
[8] D. Ratan, T. Jiang, D. A. Barkhouse, W. Xihua, G. P.-A. Andras, B. Lukasz, L. Larissa, E. H. Sargent, *J. Am. Chem. Soc.* **2010**, *132*, 5952.
[9] J. M. Luther, J. Gao, M. T. Lloyd, O. E. Semonin, M. C. Beard, A. J. Nozik, *Adv. Mater.* **2010**, *22*, 3704.
[10] J. Gao, J. M. Luther, O. E. Semonin, R. J. Ellingson, A. J. Nozik, M. C. Beard, *Nano Lett.* **2011**, *11*, 1002.
[11] D. A. R. Barkhouse, R. Debnath, I. J. Kramer, D. Zhitomirsky, A. G. Pattantyus-Abraham, L. Levina, L. Etgar, M. Grätzel, Edward H. Sargent, *Adv. Mater.* **2011**, *23*, 3134.
[12] K. S. Leschikies, T. J. Beatty, M. S. Kang, D. J. Norris, E. S. Aydil, *ACS Nano* **2009**, *3*, 3638.
[13] L. Etgar, W. Zhang, S. Gabriel, S. G. Hickey, M. K. Nazeeruddin, A. Eychmüller, B. Liu, M. Grätzel, *Adv. Mater.* **2012**, *24*, 2202.
[14] L. Etgar, T. Moehl, S. Tscharntke, S. G. Hickey, A. Eychmüller, M. Grätzel, *ACS Nano* **2012**, *6*, 3092.
[15] A. G. Pattantyus-Abraham, I. J. Kramer, A. R. Barkhouse, X. Wang, G. Konstantatos, R. Debnath, L. Levina, I. Raabe, M. K. Nazeeruddin, M. Gratzel, E. H. Sargent, *ACS Nano* **2010**, *4*, 3374.
[16] J. B. Sambur, T. Novet, B. A. Parkinson, *Science* **2010**, *330*, 63.
[17] O. E. Semonin, J. M. Luther, S. Choi, H.-Y. Chen, J. Gao, A. J. Nozik, M. C. Beard, *Science* **2011**, *334*, 1530.
[18] C. M. Evans, L. Guo, J. J. Peterson, S. Maccagnano-Zacher, T. D. Krauss, *Nano Lett.* **2008**, *8*, 2896.
[19] M. V. Kovalenko, D. V. Talapin, M. A. Loi, F. Cordella, G. Hesser, M. I. Bodnarchuk, W. Heiss, *Angew. Chem. Int. Ed.* **2008**, *47*, 3029.
[20] M. Lazzeri, A. Vittadini, A. Selloni, *Phys. Rev. B* **2001**, 63.
[21] S. A. Ivanov, A. Piryatinski, J. Nanda, S. Tretiak, K. Zavadil, W. O. Walalce, D. Werder, V. I. Klimov, *J. Am. Chem. Soc.* **2007**, *129*, 11708.
[22] A. Piryatinski, S. A. Ivanov, S. Tretiak, V. I. Klimov, *Nano Lett.* **2007**, *7*, 108.
[23] D. Oron, M. Kazes, U. Banin, *Phys. Rev. B* **2007**, *75*, 035330.
[24] Q. Dai, Y. Wang, X. Li, Y. Zhang, D. J. Pellegrino, M. Zhao, B. Zou, J. T. Seo, Y. Wang, W. W. Yu, *ACS Nano* **2009**, *3*, 1518.
[25] O. Madelung, *Semiconductors: Data Handbook*, Heidelberg, Germany, Springer **2004**.
[26] I. Kang, F. W. Wise, *J. Opt. Soc. B* **1997**, *14*, 1632.
[27] R. Vaxenburg, E. Lifshitz, *Phys. Rev. B* **2012**, *85*, 075304.
[28] G. I. Maikov, R. Vaxenburg, A. Sashchiuk, E. Lifshitz, *ACS Nano* **2010**, *4*, 6547.
[29] D. Yanover, R. K. Capek, A. R. Brusilovski, R. Vaxenburg, N. Grumbach, G. I. Maikov, O. Solomeshch, A. Sashchiuk, E. Lifshitz, *Chem. Mater.* **2012**, *24*, 4417.
[30] X. Han, Q. Kuang, M. Jin, Z. Xie, L. Zheng, *J. Am. Chem. Soc.* **2009**, *131*, 3152.